Biomimetic nanocrystalline apatite coatings synthesized by Matrix Assisted Pulsed Laser Evaporation for medical applications

Anita Ioana Visan, David Grossin, Nicolaie Stefan, Liviu Duta, Floralice Marimona Miroiu, George E. Stan, Mihai Sopronyi, Catalin Luculescu, Michèle Freche, Olivier Marsan, et al.

Biomimetic nanocrystalline apatite coatings synthesized by Matrix Assisted Pulsed Laser Evaporation for medical applications

A. Visan[a], D. Grossin[b], N. Stefan[a], L. Duta[a], F.M. Miroiu[a], G.E. Stan[c], M. Sopronyi[a], C. Luculescu[a], M. Freche[b], O. Marsan[b], C. Charvilat[b], S. Ciuca[d], I.N. Mihailescu[a,*]

[a] National Institute for Lasers, Plasma, and Radiation Physics, 409 Atomistilor Street, RO-77125, MG-36, Magurele-Ilfov, Romania
[b] CIRIMAT – Carnot Institute, University of Toulouse, ENSIACET, 4 Allée Emile Monso, 31030 Toulouse Cedex 4, France
[c] National Institute of Materials Physics, RO-077125, Magurele-Ilfov, Romania
[d] Politehnica University of Bucharest, Faculty of Materials Science and Engineering, Bucharest, Romania

A B S T R A C T

We report the deposition by Matrix Assisted Pulsed Laser Evaporation (MAPLE) technique of biomimetic nanocrystalline apatite coatings on titanium substrates, with potential application in tissue engineering. The targets were prepared from metastable, nanometric, poorly crystalline apatite powders, analogous to mineral bone, synthesized through a biomimetic approach by double decomposition process. For the deposition of thin films, a KrF* excimer laser source was used ($\lambda = 248$ nm, $\tau_{FWHM} \leq 25$ ns). The analyses revealed the existence, in synthesized powders, of labile non-apatitic mineral ions, associated with the formation of a hydrated layer at the surface of the nanocrystals. The thin film analyses showed that the structural and chemical nature of the nanocrystalline apatite was prevalently preserved. The perpetuation of the non-apatitic environments was also observed. The study indicated that MAPLE is a suitable technique for the congruent transfer of a delicate material, such as the biomimetic hydrated nanohydroxyapatite.

Keywords:
Biomimetic hydrated bioapatites
Thin films
Matrix Assisted Pulsed Laser Evaporation (MAPLE)
Coated implants

1. Introduction

In recent years, a considerable attention was paid to the development of implants with bioactive fixation [1,2]. Nowadays biomedical research aims for the increase of surface biocompatibility of titanium (Ti) orthopedic or dental implants by the coating with biologically active materials. Ti stands for the metallic material of choice in reconstructive medicine due to its excellent mechanical properties in bulk, relative to the low mass density, and high corrosion resistance [3].

Calcium phosphate (CaP) ceramics are currently the most used biomaterials for metal implant coatings in order to increase the osseoconductivity and overall bioactivity, thus speeding up the biointegration and repairing process of bones or other hard tissues [4]. Nevertheless, recent studies have shown that the actual bioapatite present in the human body is generally nonstoichiometric and much more bioactive than pure hydroxyapatite [HA, $Ca_{10}(PO_4)_6(OH)_2$], which is considered the model for the basic constituent of the inorganic part of the bone (65–75 wt.%, depending on age and sex) [5,6]. The mineral part of bone is in fact a hydrated calcium-deficient apatite of low crystalline status, containing several ion substitutions: Na^+, Mg^{2+} can substitute Ca^{2+} ions; $(CO_3)^{2-}$ and $(HPO_4)^{2-}$ ions can substitute phosphate ions; $(CO_3)^{2-}$, Cl^- and F^- can replace hydroxyl ions, as well as other various trace elements (Zn, Al, Sr) [7,8].

Research efforts have been therefore focused on the synthesis of bioapatite materials as close as possible to the human bone composition and structure, and their next congruent transfer onto the surface of metallic implants [1,9,10]. Various doping and different methods of deposition have been employed in the past in the attempt of obtaining a suitable apatitic structure. We thus mention: pulsed laser deposited magnesium, manganese or strontium doped HA coatings [11–13], magnetron sputtered B-type carbonated HA thin films [14], and manganese, strontium or fluorine (co)-doped electrodeposited HA layers [15–18].

One important issue emerging during many physical deposition studies is the highly dehydrated nature of the fabricated HA films (thus, contrasting to the actual mineral phase of bone), because of high vacuum deposition conditions, high temperature process, or volatility of OH^- species. The chemical deposition techniques can surpass this drawback, but are generally leading to films with poor adhesion [19,20].

In this context, the apatite nanocrystals obtained by precipitation methods in solution present physico-chemical features similar

* Corresponding author. Tel.: +40 21 457 44 91; fax: +40 21 457 42 43.
E-mail address: ion.mihailescu@inflpr.ro (I.N. Mihailescu).

http://dx.doi.org/10.1016/j.mseb.2013.11.007

to those of bone nanocrystals, which make them very promising biomaterials for the preparation of highly bioactive ceramics [21]. Non-stoichiometric nanocrystalline apatite-based biomaterials mimic the mineral bone crystal structure and composition and exhibit a controlled reactivity in respect to the interactions with components of biological fluids (ions, proteins) [22]. Recently, apatite nanocrystals have been tested as coatings and they have shown superior biological behavior [23]. One significant property is their surface reactivity that is related to the existence of a metastable hydrated layer on the surface of the nanocrystals in powders [5]. The synthesis process of nanocrystalline apatites poorly crystallized by conventional techniques, at high temperature, strongly alters their physico-chemical characteristics and biological properties. The synthesis processes used in this paper were therefore aimed to limit these alterations (as grain growth, dehydration, evolution toward stoichiometry) [24].

We emphasize upon the advantages for processing the powders at low temperature and illustrate the effect of experimental parameters' synthesis on apatite powder characteristics. The non-stoichiometric nanocrystalline apatite bioceramic coatings were deposited on Ti substrates by Matrix Assisted Pulsed Laser Evaporation (MAPLE) technique, considered convenient for the well-protective transfer of novel organic delicate molecules thin films [25,26]. MAPLE ensures good thickness control, patterning facility, and is appropriate for a wide range of biomaterials prone to the decomposition and degradation under direct intense laser irradiation and subsequent exposure to plasma action [25–27]. One can deposit patterned films on a variety of substrate materials with different geometric shapes. The most important requirement of MAPLE process is to minimize and possibly avoid the photonic damage, either of the film or of matrix material during laser interaction and transfer [25–27]. MAPLE is a non-contact deposition technique, which eliminates major sources of contamination and can be integrated with other sterile processes [25–27].

This manuscript it is dedicated to the deposition by MAPLE technique of biomimetic nanocrystalline apatite coatings on titanium substrates, with potential applications in medicine. The key part of the reported evidence is the investigation of the labile non-apatitic environments of mineral ions associated with the high surface reactivity of biomimetic apatites which was studied in our previous work [28].

2. Materials and methods

2.1. Synthesis of biomimetic apatite powders

Biomimetic apatites (BmAp), with complex chemical formula $Ca_{10-x+u}(PO_4)_{6-x-y}(HPO_4{}^{2-})_{x+y}(OH)_{2-x+2u+y}$, $0 \le x \le 2$ and $0 \le 2u + y \le x$ [28], were synthesized at room temperature (RT) and physiological pH by double decomposition method between a di-ammonium hydrogen phosphate and a calcium nitrate tetrahydrate solution [120 g of $(NH_4)_2HPO_4$ (Carlo Erba, analysis quality: purity: 98%) in 1500 ml of deionised water, 52.2 g of $Ca(NO_3)_2{\cdot}4H_2O$ (Merck, analysis quality: purity: 99%) in 750 ml of deionised water]. The calcium solution was rapidly poured into the phosphate solution at 20 °C and stirred for 10 min. The excess of phosphate ions was designed to fix the pH buffering at a homeostatic value of 7.4, which remain constant throughout the synthesis process. After maturation for one day, the precipitates were filtered under vacuum and washed with deionised water. Then, the gel was freeze-dried and stored in a freezer to prevent further maturation of the BmAp nanocrystals. The chosen conditions (physiological pH of 7.4 in close resemblance to human body) resulted in the synthesis of a poorly crystalline apatite analogous to the mineral part of neo-formed bone.

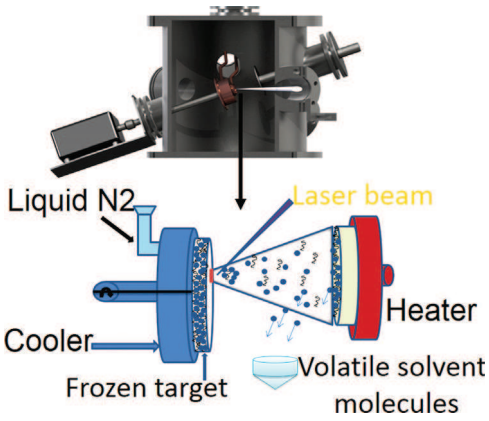

Fig. 1. MAPLE experimental set-up.

2.2. Deposition of BmAp thin films

The MAPLE set-up used in experiments is depicted schematically in Fig. 1.

Thin BmAp films have been deposited using a KrF* excimer laser source ($\lambda = 248$ nm, $\tau_{FWHM} \le 25$ ns), running at a repetition rate of 10 Hz. The commonly used substrates in experiments were disks of pure Ti of 1.2 cm in diameter and 0.2 cm in thickness (Dentaurum GmbH). For microscopic characterizations, some structures were deposited on ⟨1 1 0⟩ single-crystalline Si wafers (MEMC Electronic Materials Inc.). All substrates were degreased in acetone and ethanol in an ultrasonic bath for 30 min and rinsed with deionized water. For MAPLE experiments, the slurry was prepared by dispersing 475 mg of BmAp, maturated for one day, in a hydro-alcoholic solution, where benzoic acid was previously dissolved. The resulting slurry was carefully stirred at RT and then poured in a stainless steel cup. The solution was next frozen at 77 K by immersion in liquid nitrogen in direct contact with a cooler inside the deposition chamber. This way, the target evaporation was initially slowed down to be finally completely stopped. The target-substrate separation distance was of 5 cm. During deposition, the targets were rotated with 0.3 Hz and translated along two orthogonal axes to avoid piercing and to ensure the deposition of a uniform film. The residual working pressure inside the deposition chamber was set at ~2.7 Pa. For the deposition of each film, 30,000 subsequent laser pulses have been applied.

The selected volatile solvent, the benzoic acid, is highly absorbing the laser wavelength in frozen state, but is not reacting with the solute even under laser exposure. According to literature, the dehydration effect of BmAp after the suspension of powder in a hydro-alcoholic solution keeps negligible [22]. A comparative study on the incident laser fluence effect was conducted. Four fluence values of 0.3 J/cm^2, 0.5 J/cm^2, 0.75 J/cm^2 and 1 J/cm^2 have been chosen and the applied criterion was the prevention of the powder decomposition. Finally, the value of 0.75 J/cm^2 was selected, as being the highest laser fluence for which the films are deposited stoichiometric and without any decomposition or denaturation of the BmAp powder, with the largest possible rate. This way, the structural and functional fidelity was preserved after MAPLE transfer, by avoiding a significant direct laser–biomaterial interaction in the deposition chamber. Due to the low concentration of solute (biomaterial) in the frozen target, the laser photons preponderantly interact with the matrix (solvent), which is vaporized [29]. The metastable BmAp molecules are released unaltered and, by means of collisions with the other molecules, are directed toward the substrate, where they form a uniform thin film. In the same time, the volatile solvent is pumped away by the vacuum system.

2.3. Characterization methods

2.3.1. Nanopowder investigation

(i) Calcium concentration in the initial powders was measured by atomic absorption spectroscopy, using a *Perkin Elmer AAnalyst 300 Atomic Absorption* spectrometer. The phosphorus concentration was determined by spectrophotometry of the phospho-vanado molybdenum complex, using a *Hitachi V-1100* spectrophotometer at 460 nm, respecting the protocol described in Ref. [30]. The chemical analysis was based on the dissolution of apatite in acidic solution before the analysis, for the calcium and orthophosphate ions control, or during the analysis, in the case of carbonate ions, respectively.

(ii) The sample characterization by X-ray diffraction (XRD) was performed using a curved counter diffractometer *INEL CPS 120* with monochromatic Co Kα radiation (λ = 1.789 Å).

(iii) Fourier transform infrared (FTIR) spectroscopy analysis of the powder was carried out in transmission mode, in the (4000–400) cm^{-1} range, with a *Perkin Elmer 1600* °C thermospectrometer with a resolution of 4 cm^{-1}. The Raman spectra of powders were recorded on a *Jobin Yvon HR 800* spectrometer, in the (3800–100) cm^{-1} range, with a laser excitation wavelength of 632.8 nm. The experimental data were fitted using the Origin software.

(iv) Transmission electron microscopy (TEM) studies were conducted on a *JEOL JEM 1011* (100–500 kV) microscope.

2.3.2. Thin film investigation

(i) Thin film thickness was measured with an *Ambios Stylus Profiler XP-2* system, having 0.1 nm vertical resolution, an optical deflection height-measurement sensor and stylus with 2.5 μm radius and 0.1 mg force.

(ii) The identification of crystalline phases was conducted by Grazing Incidence X-ray Diffraction (GIXRD) using a *Bruker D8 Advance diffractometer*, in parallel beam setting, equipped with Cu target X-ray tube. The incidence angle was set at 2°, and the scattered intensity was scanned in the range 20–50° (2θ), with a step size of 0.04°, and 100 s per step.

(iii) The FTIR spectroscopy analysis of the thin films was performed with a *Perkin Elmer BX Spectrum* spectrometer, in attenuated total reflection (ATR) mode using a *Pike-MIRacle* diamond head of 0.18 cm diameter. The spectra were recorded in the range (4000–550) cm^{-1}, with a resolution of 4 cm^{-1} and a total of 150 scans per experiment.

(iv) The Raman measurements were made with the same system used for the nanopowder characterization.

(v) The morphology of the films was examined by scanning electron microscopy (SEM) with a *FEI Inspect S* electron microscope, operating at 20 kV acceleration voltage, in high vacuum, under secondary electron mode. Cross-section SEM images were recorded on a specimen deposited on Si wafers in identical conditions in order to investigate the film homogeneity in depth. Additionally, higher resolution morphological studies were performed by atomic force microscopy (AFM), using an *Agilent* 5500 apparatus equipped with a supersharp *TESP-SS Nanoworld* tip (nominal resonance frequency 320 kHz and nominal radius curvature 2 nm).

(vi) The Ca/P ratio of the thin apatitic films was determined by energy dispersive spectroscopy (EDS) analysis, using *EDAX Inc.* instrument with a SiLi detector, operated at 20 kV. The analyses were performed on five relatively large regions of 250 μm × 250 μm, in order to ensure the good statistic of the measurement.

(vii) The HA films adherence to the substrate was tested by pull-out method. The experimental procedure was conducted in accordance with the ASTM D4541 and ISO 4624 standards. The investigations were carried out using a *DFD Instruments AT101 PAT MICRO* adhesion tester equipped with a 0.28 cm diameter stainless steel test elements (dollies), glued to films surface with a cyano-acrylate one-component *Epoxy* adhesive, E1100S. After gluing, the samples were placed in an oven for thermal curing (130 °C/1 h). Each test element was pulled-out vertically with a calibrated hydraulic pump until detachment. The bonding strength values were calculated as the ratio between the pulling force at which the adhesive fracture of the HA film occurred to the actually film delaminated area. We mention that prior to the film testing, control measurements regarding the quality of the bonding adhesive (steel-on-steel) were performed. The average adherence value estimated at the stainless steel dolly/stainless substrate interface was of ~85 MPa.

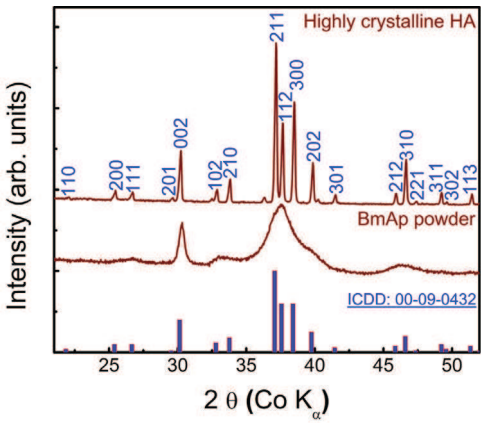

Fig. 2. XRD patterns of stoichiometric crystalline HA and BmAp powder.

3. Results and discussion

3.1. Nanopowders' characterization

From the concentration of calcium and phosphate ions, obtained by chemical analyses, we inferred the Ca/P atomic ratio in order to assess the chemical composition of synthetic BmAp after one day of maturation. The obtained Ca/P atomic ratio value of 1.5 is noticeably inferior to the theoretical value of 1.67, characteristic to stoichiometric HA. This puts in evidence the non-stoichiometric, calcium-deficient, biological-like nature of the apatitic (HA) phase used in our experiments.

The XRD powder patterns of a crystalline pure commercial powder HA (Tecknimed SA) and of the synthetic nanocrystalline apatite maturated for one day are presented comparatively in Fig. 2. Both materials exhibited the characteristic lines of the hexagonal HA phase (ICDD: 00-009-0432), with sharp and well defined peaks in the case of commercial crystalline material, and large and overlapping maxima in the case of BmAp maturated powder. The broadening of the BmAp peaks is the indicative of a poorly crystallized nanoapatite, due to the lattice disorder and very fine size of crystallites, similarly to mineral bone [31,32].

The mean crystallite size was derived using the well-known Scherrer equation [33]:

$$L_{hkl} = \frac{K * \lambda}{b * \cos\theta}$$

Here L_{hkl} is the mean size of the ordered (crystalline) domains, which may be smaller or equal to the grain size; shape factor $K = 0.94$; λ is the X-ray wavelength; β is the line broadening at

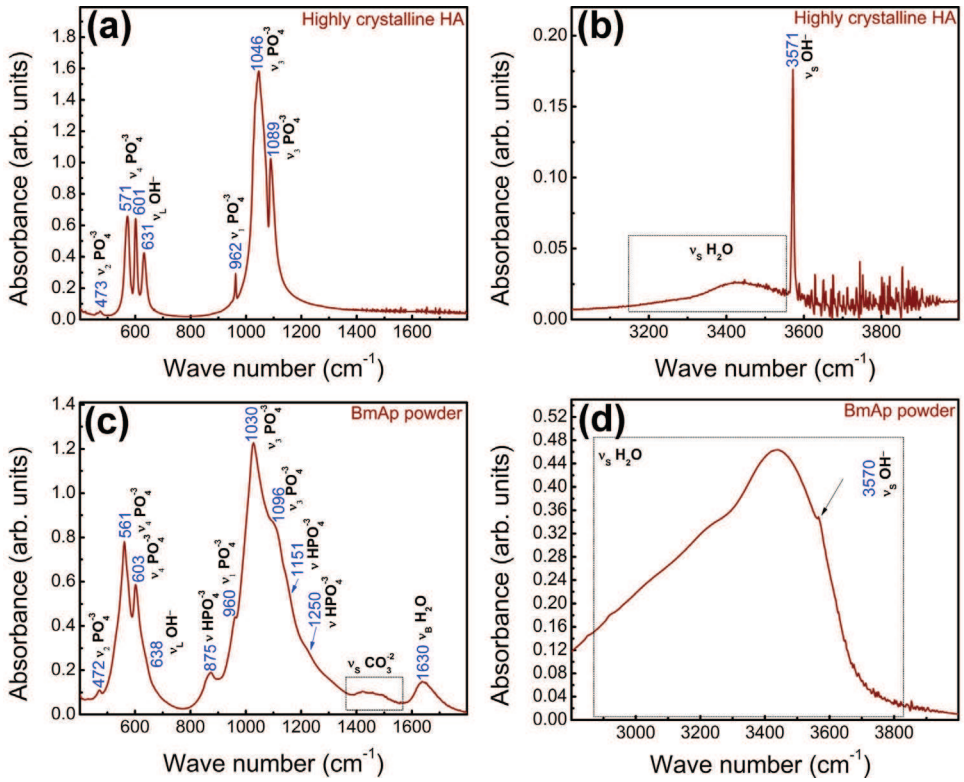

Fig. 3. FTIR spectra of highly crystalline HA (a and b) and BmAp powders (c and d) in the spectral regions: 1800–400 cm^{-1} (a and c) and 4000–2800 cm^{-1} (b and d).

half the maximum intensity, after subtracting the instrumental line broadening, in radians; and θ is the Bragg angle.

It was applied to diffraction lines (0 0 2) and (3 1 0), giving estimated values of the crystallite length and an average of their width. Thus, if one ignores the strain effects, basic profile analysis leads to L_{002} values of ~20 nm, and L_{310} of ~5 nm, for a maturation time of one day. These data confirmed the nanometer size of the crystallites constitutive of BmAp powder, and indicated their elongated shape. It should be noted that previous studies revealed by insightful morpho-structural analyses that human bone also exhibits an elongated crystallite shape, having an anisotropic growth along the [*0 0 l*] crystallographic direction [34,35]. FTIR spectrum is given in Fig. 3 of the BmAp powder (c and d), together with the one of the stoichiometric crystalline HA (a and b), in the fingerprint (1800–400 cm^{-1}) and functional group (4000–2800 cm^{-1}) regions. All the characteristic absorption bands of HA are present. The phosphate band positions correspond to the ones often reported in specialized literature (for stoichiometric HA) [36–39]. The prominent phosphates bands are visible [472 (ν_2 bending mode of PO_4^{3-} groups), 561 and 603 (ν_4 asymmetric bending of PO_4^{3-} groups), 875 (P–O–H vibration in the HPO_4^{2-} group), 960 (ν_1 symmetric stretching of PO_4^{3-} groups), 1030–1096 (ν_3 asymmetric stretching of PO_4^{3-} groups), 1151 (vibrations of HPO_4^{2-} ions), and 1250 cm^{-1} (vibrations of HPO_4^{2-} ions and possible $(PO_2)^-$ (Q^2) species)]. The structural OH^- shallow bands at 638 cm^{-1} (libration mode) and 3570 cm^{-1} (stretching mode) were also evidenced (Fig. 3c and d). Additionally, one observes the presence of the broad water bands at (3400–3000) cm^{-1} (stretching mode) and 1630 cm^{-1} (bending mode), which indicate a higher degree of hydratation of the material. The broad ν_3 CO_3^{2-} asymmetric stretching band peaking at ~1450 cm^{-1} suggests the slight carbonation of the BmAp powder, due to contamination during preparation or handling.

All IR bands of BmAp powder (Fig. 3c) are broader and less conspicuous than the corresponding ones of the stoichiometric HA (Fig. 3a), pointing to the lower structural ordering of this compound, in good agreement with the XRD observations (Fig. 2).

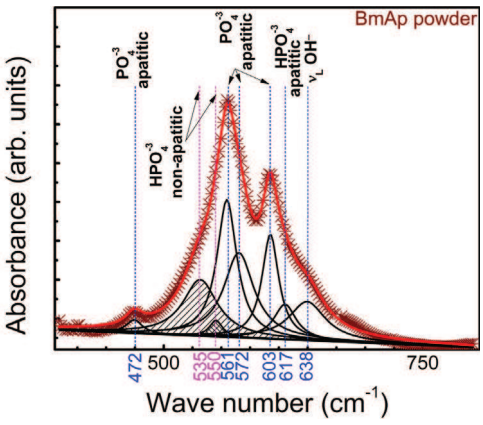

Fig. 4. Curve fitting of ν_4 $(PO_4)^{3-}$ IR band of BmAp powder.

Moreover, the FTIR bands of the BmAp powder have complex shapes suggesting the overlap of various vibration contributions. The identification of the BmAp sub-structure was attempted by the curve fitting of the ν_4 PO_4^{3-} asymmetric bending domain (Fig. 4). Besides the triply degenerated bands of ν_4 PO_4^{3-} groups (561, 572 and 603 cm^{-1}), the HPO_4^{2-} band (617 cm^{-1}), and the libration mode of OH^- (638 cm^{-1}) [37], disclosed the presence of additional bands, positioned at 535 and 550 cm^{-1}. They belong to the P—O bonds, which are not usually present in an apatitic structure and cannot be assigned to an apatitic environment [22,28,36]. The formation of non-apatitic environments is associated to the synthesis of apatite nanocrystals at physiological pH in close resemblance to human bone [36].

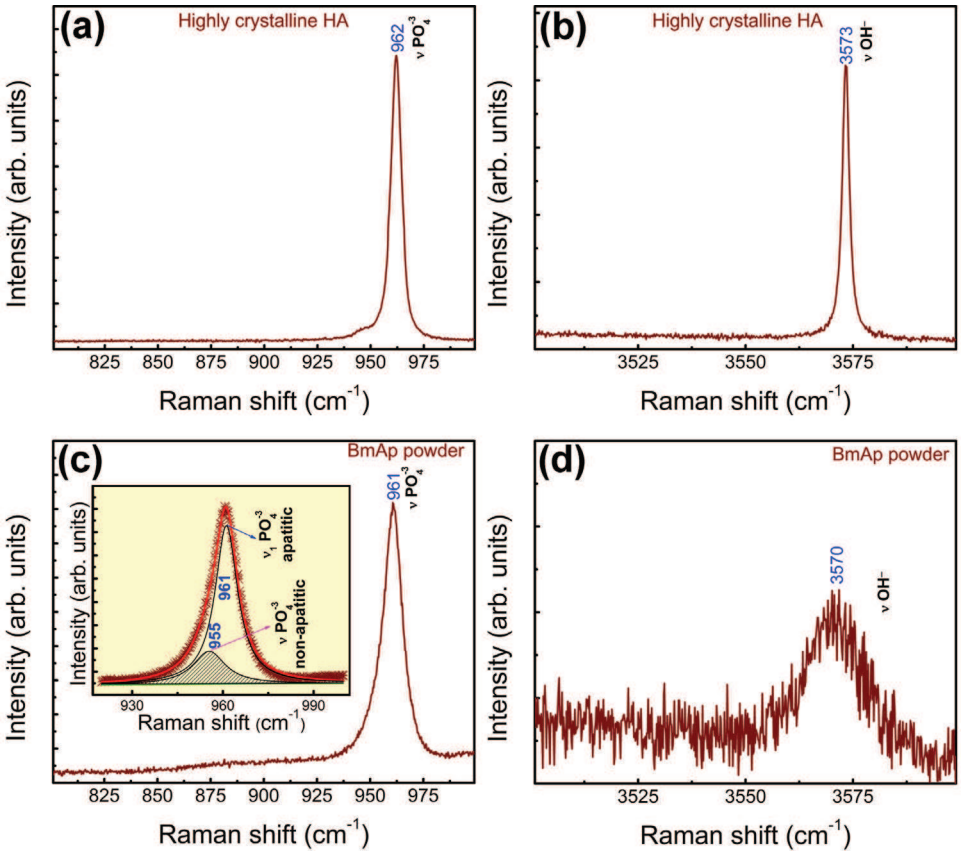

Fig. 5. Raman spectra of highly crystalline HA (a and b) and BmAp powder (c and d) in the spectral regions of ν_1 $(PO_4)^{3-}$ (a and c) and ν_S $(OH)^-$ (c and d) bands. *Insert*: Curve fitting of ν_1 $(PO_4)^{3-}$ Raman band of BmAp powder.

The Raman investigations (Fig. 5) were in agreement with the FTIR results (Figs. 3 and 4), and were used to get additional information on the chemical composition and structure of BmAp powder. If in the case of the pure HA crystalline powder a symmetrical peak is evidenced (at 962 cm^{-1}), due to the ν_1 PO_4^{3-} vibrations, for the BmAp powder the analogous peak had an asymmetric allure, hinting toward a mix bands contribution. The curve fitting evidenced two distinct components (see Fig. 5c-inset): an intense one at 961 cm^{-1} (which can be attributed to apatitic PO_4), and a weak one at 955 cm^{-1} (assignable to non-apatitic phosphate groups). They arise because of the significant differences in the intertetrahedron P—O bond lengths between the respective groups. Such bands are not observable in case of well crystallized stoichiometric apatites. The presence of ν OH^- structural vibrations was noticed at ~3571 cm^{-1} for both crystalline HA and BmAp powders (Fig. 5b and d)

The agglomeration of acicular grains having (150–250) nm in length and (10–15) nm in width were revealed by TEM (Fig. 6). The TEM analyses indicated the homogeneous crystalline morphology of the BmAp powder, and confirmed its nanometric nature.

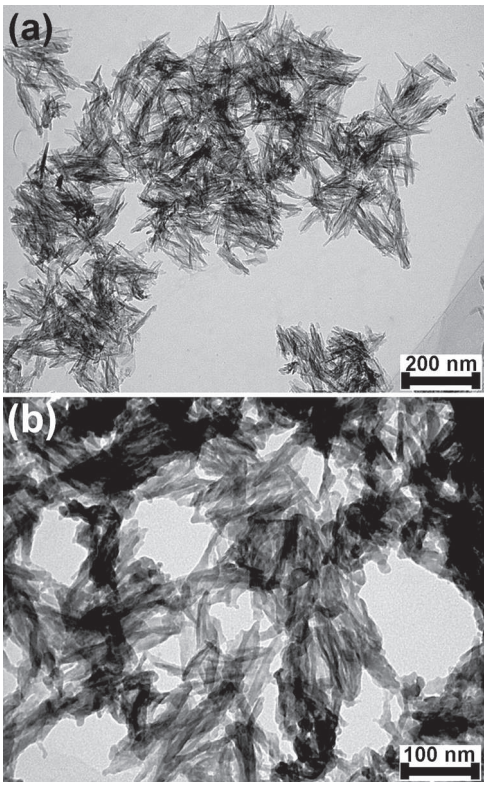

Fig. 6. TEM micrographs of BmAp powder collected at two magnifications (a: bar = 200 nm; b: bar = 100 nm).

3.2. *Characterization of deposited thin films*

The AFM and step profilometry measurements indicated that the BmAp MAPLE films had an average thickness of ~1.55 ± 0.15 μm.

The cross-view (Fig. 7a) and top-view (Fig. 7b) SEM micrographs indicated that the films had a rather uniform, homogeneous and fairly compact morphology, both in depth and on the surface. The film surface consists of nanograins hard to discriminate, characteristic to films deposited by MAPLE technique [26,27]. Next, the

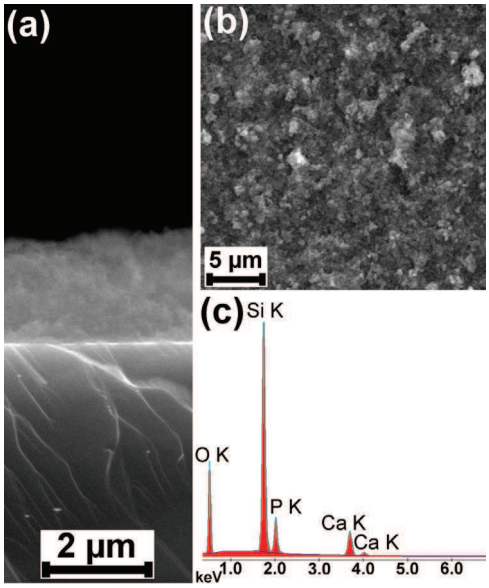

Fig. 7. SEM micrographs recorded in cross-view (a) and top-view modes (b) for the BmAp MAPLE film. EDS spectrum for the BmAp MAPLE film (c).

film morphology was investigated in more detail by high resolution AFM. Fig. 8 presents the films microstructure as visualized by phase-contrast AFM. These results supports the homogenous character of the nanostructured MAPLE film, consisting predominantly of fairly packed grains with sizes in the range of 30–50 nm. However, rare local surface abnormalities were observed (Fig. 8c), consisting of clusters of significantly larger grains (150–200 nm) with round edges. The presence of nanoparticulates, is characteristic to structures deposited by pulsed laser technologies (PLD and MAPLE) [4,27], and can be seen as advantageous in the particular case of coated implants due to the greater interaction of the active surface with the surrounding cells.

The EDS qualitative analysis confirmed the uniform distribution of calcium and phosphorous throughout the film (data not shown), whilst the EDS spectrum (Fig. 7c) indicated the absence of impurities. The quantitative EDS analysis revealed a Ca/P ratio of 1.48 ± 0.07, close to the one of the starting powder.

The short-range order was studied by FTIR and Raman spectroscopies, whilst the long-range order was investigated by GIXRD.

The spectroscopic investigations put in evidence the preservation, after deposition, of the non-apatitic environments which are believed to enhance the surface reactivity, as mentioned in Ref. [36]. The FTIR (Fig. 9) and Raman (Fig. 10) spectra of the BmAp MAPLE films were quite similar to the analogous spectra of the starting powder.

Unlike the IR spectrum of the BmAp powder (Fig. 3c), one can notice in the FTIR fingerprint region of the MAPLE film (Fig. 9a and c) better defined and sharper bands, which designate a higher structural order. This allowed for a better discrimination of the film "sub-structure". The shallow phosphate band (at $\sim$552 cm^{-1}) associated with the hydrated layer covering the nanocrystals [22,28,36], assigned to the non-apatitic chemical environments [22,36] and previously hinted by the IR powder spectrum fitting (Fig. 4), is observed rather distinctively for the deposited film, along with all the other typical apatitic vibrations, revealed in case of the BmAp powder (see Figs. 4 and 9a, b). The other non-apatitic vibration band (positioned in the case of the powder at $\sim$535 cm^{-1}, Fig. 4), could not be evidenced, as infrared spectrum in ATR mode is limited to the cut-off point at 550 cm^{-1}, where the diamond window absorbs the infrared radiation. The shift of the OH^- libration band (Figs. 3c and 9a), relative to its position seen for the

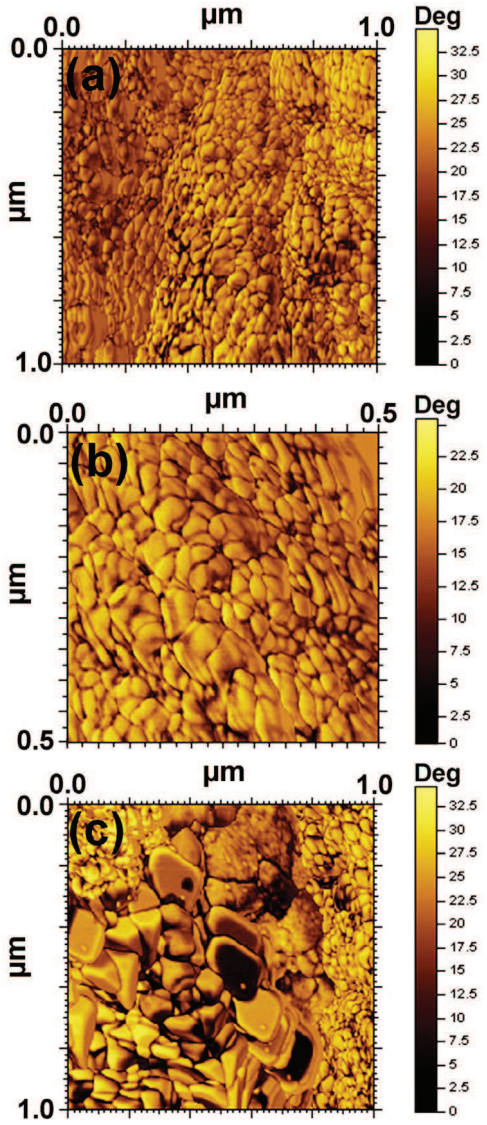

Fig. 8. AFM phase-contrast images of BmAp MAPLE film recorded in the intermittent contact mode, at different scales: 1 μm × 1 μm (a and b); 0.5 μm × 0.5 μm (b), on different surface regions.

stoichiometric HA powder (Fig. 3a), suggests that these structural units are more disordered in case of BmAp materials, their locations in the "OH channel" being altered. A slight carbonation of the film has been also noticed (as a broad band centered at $\sim$1450 cm^{-1}).

The Raman spectrum (Fig. 10) of the deposited film displayed a similar asymmetric envelope as the one seen for the BmAp parent powder (Fig. 5c), therefore suggesting its intimate structural resemblance.

The GIXRD pattern (Fig. 11) of the MAPLE film indicated the presence of HA (ICDD: 00-009-0432) as a single low crystalline phase, but with a slightly improved structural order in respect with the BmAp powder, which is in agreement with the aforementioned ATR-FTIR observations. Crystallite sizes estimated at the (0 0 2) and (3 1 0) crystal planes, by applying the Scherrer equation, were also higher ($L_{002} \approx 45$ nm, and $L_{002} \approx 7$ nm). The formation of amorphous calcium phosphate (ACP), is kinetically possible at pH higher than 7, although the HA is the most thermo-dynamically stable phase. The minor presence of ACP should not be disregarded, and could also account for the systematic bands shifts of BmAp materials relative to the stoichiometric HA IR peaks' positions (Figs. 3 and 9), as well as for their slightly lower Ca/P ratios.

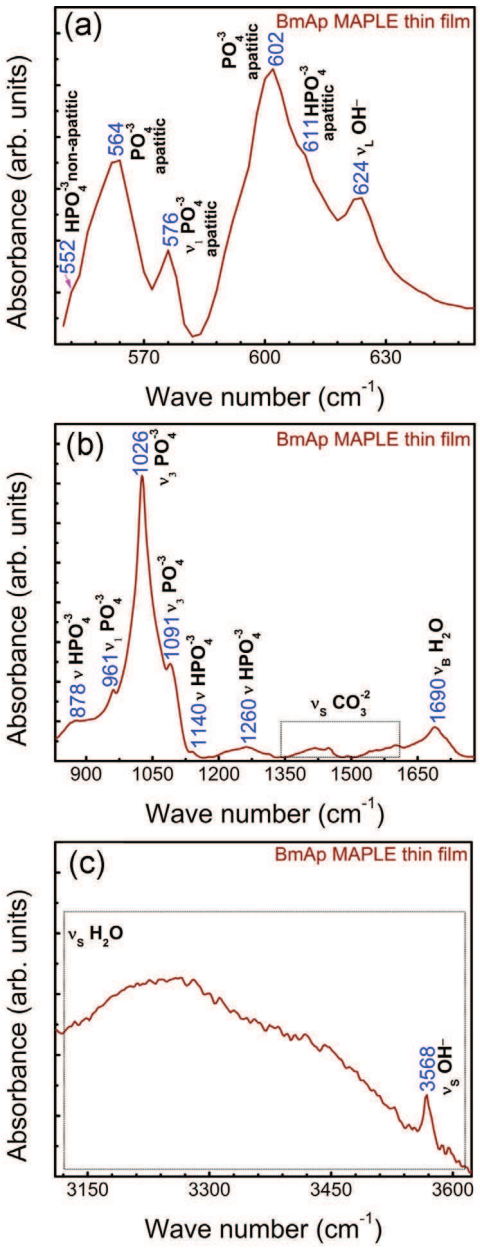

Fig. 9. FTIR spectra of the BmAp MAPLE thin film in the spectral regions: 650–550 cm^{-1} (a), 1800–830 cm^{-1} (b), and 3620–3100 cm^{-1} (c).

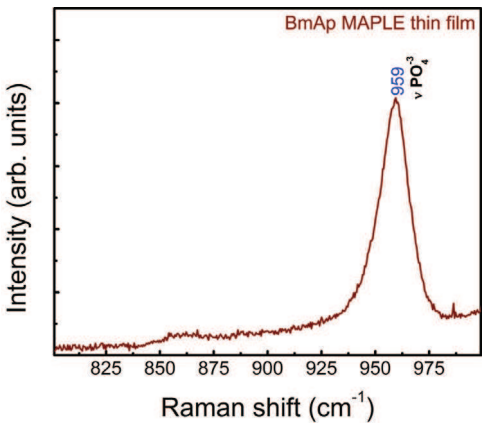

Fig. 10. Raman spectrum of the BmAp MAPLE thin film in the spectral region of ν_1 $(PO_4)^{3-}$.

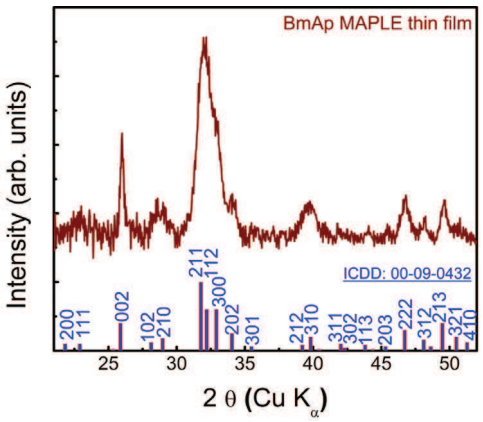

Fig. 11. GIXRD pattern of the BmAp MAPLE thin film.

The adherence value at the BmAp film/substrate interface was of 44 ± 5.3 MPa, as estimated by the pull-out measurements, thus, close to the one (~50 MPa) imposed by the international standards for load bearing implant HA coatings [40].

Our results demonstrated the congruent transfer of the BmAp material by MAPLE technique, the obtained films preserving the chemical composition of the parent powder, with only a slight alteration of the initial nanocrystals.

The link between the HA bioreactivity and the presence of hydrated layer has been proposed in the past [22,36,41]. This superficial layer can intermediate various interactions (as *e.g.*: proteins bonding or adsorption, ionic exchanges or sharing) with the biological environment [22,36,41]. On the other part, the OH content can influence the *in vivo* degradability of the HA material, as the osteoclasts are known to induce a local drop of the pH to be able to resorb the apatite [42]. The low concentration of OH can result in a reduced buffering capability of the material, favoring its dissolution and resorbtion by osteoclasts [41,42]. Neverthless, a too low OH concentration can induce a fast solubilization of the HA coating, which can drastically reduce the implant's functionality. It should be mentioned that a higher concentration of hydroxyl groups can lead to a slower rate of dissolution, and also enables the buffering capacity of the implant for specific medical applications performing in highly acidic media (*e.g.* dentistry) [41,43].

4. Conclusions

We performed the deposition of adherent biomimetic nanocrystalline apatite thin films by MAPLE technique onto titanium and silicon substrates.

The FTIR and Raman spectra of the thin films were found to be highly similar and had an identical signature to the spectrum of the initial powder. The observed shoulders attributed to the HPO_4^{2-} non-apatitic ions confirm the preservation of a hydrated phase inside the thin films.

A very limited transformation of the initial nanocrystals was observed, whilst the original chemical composition of the starting powders was preserved. The BmAp biomaterials in the form of thin films showed a high resemblance to the human hard tissue mineral structure and composition, and are therefore expected to insure a better functionality to metallic implant coatings.

We conclude that the MAPLE method is capable to maintain the structural fidelity after transfer of biomimetic apatite from a solid frozen target to a nearby substrate, in form of thin film. We have thus obtained and put in evidence the complete transfer of a hydrated, delicate material by MAPLE.

To the best of our knowledge, this is the first report of MAPLE deposition of thin films of poor-crystallized hydrated apatites

synthesized by the biomimetic method. We foresee that the characteristic features – such as composition, structure and adherence – of BmAp thin films could be tailored in the next future by optimizing the deposition parameters, to thoroughly demonstrate that the MAPLE technique is a promising alternative for fabrication of metallic implant coatings.

Acknowledgements

This research was partially supported by Executive Unit for Financing Higher Education, Research, Development and Innovation (*UEFISCDI*) of Romania under the ID 304/2011 and PCCA 153/2012 Contracts. AV also acknowledges the support of *Socrates* fellowship. GES acknowledges with thanks the financial support of PNII-RU-TE-2011-3-0164 (TE 49/2011) research grant.

References

[1] R.A. Surmenev, Surf. Coat. Technol. 206 (2012) 2035–2056.
[2] A. Sola, D. Bellucci, V. Cannillo, A. Cattini, Surf. Eng. 27 (2011) 560–572.
[3] C. Oldani, A. Dominguez, in: S. Fokter (Ed.), Recent Advances in Arthroplasty, InTech, Rijeka, 2012, pp. 149–162 (Chapter 9).
[4] V. Nelea, M. Jelínek, I.N. Mihailescu, in: R. Eason (Ed.), Pulsed Laser Deposition of Thin Films: Applications-lead Growth of Functional Materials, Wiley & Sons, New Jersey, 2006 (Chapter 18).
[5] S.V. Dorozhkin, Materials 2 (2009) 1975–2045.
[6] I.N. Mihailescu, C. Ristoscu, A. Bigi, I. Mayer, in: A. Miotello, P.M. Ossi (Eds.), Laser-Surface Interactions for New Materials Production Tailoring Structure and Properties, Springer Series in Materials Science, New York, 2010.
[7] M.M. Figueiredo, J.A.F. Gamelas, A.G. Martins, in: T. Theophile (Ed.), Infrared Spectroscopy – Life and Biomedical Sciences, Intech, Rijeka, 2012, pp. 315–338.
[8] F. Miculescu, G.E. Stan, L.T. Ciocan, M. Miculescu, A. Berbecaru, I. Antoniac, Dig. J. Nanomater. Biostr. 7 (2012) 1667–1677.
[9] B. León, J.A. Jansen, Materials Science Chemistry, Springer, New York, 2009.
[10] L. Duta, F.N. Oktar, G.E. Stan, G. Popescu-Pelin, N. Serban, C. Luculescu, I.N. Mihailescu, Appl. Surf. Sci. 265 (2013) 41–49.
[11] W. Mróz, A. Bombalska, S. Burdyńska, M. Jedyński, A. Prokopiuk, B. Budner, A. Ślósarczyk, A. Zima, E. Menaszek, A. Ścisłowska-Czarnecka, K. Niedzielski, J. Mol. Struct. 977 (2010) 145–152.
[12] E. György, P. Toricelli, G. Socol, M. Iliescu, I. Mayer, I.N. Mihailescu, A. Bigi, J. Werckman, J. Biomed. Mater. Res. A 71 (2004) 353–358.
[13] C. Capuccini, P. Torricelli, F. Sima, E. Boanini, C. Ristoscu, B. Bracci, G. Socol, M. Fini, I.N. Mihailescu, A. Bigi, Acta Biomater. 4 (2008) 1885–1893.
[14] L.E. Sima, G.E. Stan, C.O. Morosanu, A. Melinescu, A. Ianculescu, R. Melinte, J. Neamtu, S.M. Petrescu, J. Biomed. Mater. Res. A 95 (2010) 1203–1214.
[15] Y. Huang, Q. Ding, X. Pang, J. Mater. Sci. Mater. Med. 24 (2013) 1853–1864.
[16] Y. Huang, Q. Ding, X. Pang, Appl. Surf. Sci. 282 (2013) 262–456.
[17] Y. Huang, Y. Yan, X. Pang, Appl. Surf. Sci. 282 (2013) 583–589.
[18] Y. Huang, Y. Yan, X. Pang, Ceram. Int. 39 (2013) 245–253.
[19] N. Hijón, M. Victoria Cabañas, J. Peña, M. Vallet-Regí, Acta Biomater. 2 (2006) 567–574.
[20] K. Cheng, C. Ren, W. Weng, P. Du, G. Shen, G. Han, S. Zhang, Thin Solid Films 517 (2009) 5361–5364.
[21] C. Rey, A. Hina, A. Tofighi, M.J. Glimcher, Cell Mater. 5-4 (1995) 345–356.
[22] D. Eichert, C. Drouet, H. Sfihi, C. Rey, C. Combes, in: J.B. Kendall (Ed.), Nanocrystalline Apatite-based Biomaterials: Synthesis, Processing and Characterization, Biomaterials Research Advances, Nova Science Publishers, New York, 2007.
[23] P. Habibovic, F. Barrere, C.A. van Blitterswijk, K. de Groot, P. Layrolle, J. Am. Ceram. Soc. 85 (2002) 517–522.
[24] R.Z. Le Geros, Clin. Mater. 14 (1993) 65–88.
[25] B.R. Ringeisen, J. Callahan, P.K. Wu, A. Pique, B. Spargo, R.A. McGill, M. Bucaro, H. Kim, D.M. Bubb, D.B. Chrisey, Langmuir 17 (2001) 3472–3479.
[26] R. Cristescu, I.N. Mihailescu, M. Jelínek, D.B. Chrisey, in: R. Kassing, P. Petkov, W. Kulisch, C. Popov (Eds.), Functionalized Thin Films & Structures Obtained by Novel Laser Processing Issues, 223, NATO Science Series by Springer, Series II: Mathematics, Physics and Chemistry, 2006, pp. 211–226.
[27] A. Pique, in: R. Eason (Ed.), Deposition of Polymers and Biomaterials Using the Matrix-Assisted Pulsed Evaporation (MAPLE) Process, Wiley-Interscience, New Jersey, 2007.
[28] D. Grossin, S. Rollin-Martinet, C. Estournes, F. Rossignol, E. Champion, C. Combes, C. Rey, C. Geoffroy, C. Drouet, Acta Biomater. 6 (2010) 577–585.
[29] B.C. Riggs, A.D. Dias, N.R. Schiele, R. Cristescu, Y. Huang, D.T. Corr, D.B. Chrisey, EMRS Bull. 36 (2011) 1043–1050.
[30] G. Charlot, Chimie Analytique Quantitative, Masson, Paris, 1974.
[31] A. Boskey, Osteoporos. Int. 14 (2003) S16–S21.
[32] S.L. Rowles, in: R.W. Fearnhead, M.W. Stack (Eds.), Studies on Non-stoichiometric Apatites, Tooth Enamel Proc. Int. Symp., John Wright & Sons, Bristol, 1965.
[33] A.L. Patterson, Phys. Rev. 56 (1939) 978–982.
[34] S. Marković, L. Veselinović, M.J. Lukić, L. Karanović, I. Bračko, N. Ignjatović, D. Uskoković, Biomed. Mater. 6 (2011) 045005.
[35] Y. Yamato, M. Matsukawa, H. Mizukawa, T. Yanagitani, K. Yamazaki, A. Nagano, IEEE Trans. Ultrason. Ferroelectr. Freq. Control. 55 (2008) 1298–1303.
[36] C. Rey, E. Strawich, M.J. Glimcher, in: D. Allemand, J.P. Cuif (Eds.), Non-Apatitic Environments in Ca-P biominerals: Implications in Reactivity of the Mineral Phase and its Interactions with Organic Matrix Constituents, Rev. Mineral. Geochem., Monaco, 1994, pp. 55–64.
[37] M. Markovic, B.O. Fowler, M.S. Tung, J. Res. Natl. Inst. Stand. Technol. 109 (2004) 553–568.
[38] A. Roy, S.S. Singh, M.K. Datta, B. Lee, J. Ohodnicki, P.N. Kumta, Mater. Sci. Eng. B 176 (2011) 1679–1689.
[39] D.P. Minh, N. Lyczko, H. Sebei, A. Nzihou, P. Sharrock, Mater. Sci. Eng. B 177 (2012) 1080–1089.
[40] ISO-13779-2, Implants for Surgery—Hydroxyapatite—Part 2: Coatings of Hydroxyapatite, 2008.
[41] J.D. Pasteris, B. Wopenk, J.J. Freeman, K. Rogers, E. Valsami-Jones, J.A.M. van der Houwen, M.J. Silva, Biomaterials 25 (2004) 229–238.
[42] S.L. Teitelbaum, Science 289 (2000) 1504–1508.
[43] G.E. Stan, D.A. Marcov, I. Pasuk, F. Miculescu, S. Pina, D.U. Tulyaganov, J.M.F. Ferreira, Appl. Surf. Sci. 256 (2010) 7102–7110.